Journal of Power Sources 196 (2011) 6898–6901

Contents lists available at ScienceDirect

Journal of Power Sources

journal homepage: www.elsevier.com/locate/jpowsour

Short communication

Effect of particle size on the phase behavior of Li-intercalated TiO_2-rutile

M.V. Koudriachova*

Department of Chemistry, University College London, Gower Street, London WC1E 6BT, UK

ARTICLE INFO

Article history:
Received 5 October 2010
Received in revised form
15 December 2010
Accepted 17 December 2010
Available online 8 January 2011

Keywords:
Anodes
Nanomaterials
Li-batteries
Computer simulations

ABSTRACT

With the aid of *ab initio* calculations, we compare the phase behavior upon lithiation of rutile particles of different sizes and morphologies. A rationale for the differences in their structural behavior is provided by combining concepts from Crystal Field Theory and semi-empirical concepts, such as bond length variation, minimal volume expansion, with accounts for the effects of diffusion and the anisotropy of the Li-distribution. It is shown that the phase behavior of spaghetti-like nano-particles differs from bulk rutile as a result of an extended single phase insertion domain and increased disorder of Li-ions. As Li-ions strive to minimize their repulsions by increasing their mutual separation a regular network of Li-ions is formed, being a precursor to the transformation of the rutile host lattice into spinel.

1. Introduction

For decades rutile structured titanium dioxide has been disregarded for applications as an anode since at normal conditions Li-uptake by polycrystalline rutile is insignificant [1]. An exception was the report of Li-insertion to high concentration at elevated temperatures [2]. Interest in this material has been sparked recently, when a high Li-uptake was observed at normal conditions for nanostructured rutile [3–8].

The striking temperature dependence of intercalation behavior of bulk rutile has been rationalized in terms of limitations imposed by diffusion of Li-ions on the observed thermodynamics of Li-insertion [9]. Using *ab initio* simulations, it was shown that the limiting step is associated with restricted access to stable Li-sites upon single phase insertion up to Li-concentrations $x = [Li]/[Ti] \sim 0.2$ due to a highly anisotropic Li-diffusion [9,10]. At elevated temperature and in small particles Li-diffusion is activated enabling access to the stable sites and intercalation occurs to much higher Li-concentrations. It appeared that diffusion controlled Li-insertion is not specific for TiO_2 rutile, but occurs in a wider range of transition metal oxides, including TiO_2-brookite [11,12], TiO_2–B (at elevated Li-concentrations [13,14]) as well as some other rutiles (MnO_2 [15], VO_2 [16]).

More recently it has been found that the phase behavior of lithiated rutile may be influenced by the shape of nano-particles [3,4,7]. While Li-intercalation into nanostructured rutile follows the bulk behavior at elevated temperature [3], the phase transformations upon lithiation of specially tailored (spaghetti-like) nano-particles are different [4–7]. In both cases, initial insertion is a single phase reaction, to $x \sim 0.2$ [2,3] and ~0.4–0.5 [4,7], respectively, which, however, is followed by a different sequence of phase transformations. While in the former case a monoclinically distorted rutile ($Li_{0.75}TiO_2$) and a layered hexagonal $LiTiO_2$ phase [2,3,17] are formed, spaghetti-like nano-particles transform to a spinel structured titanate ($Li_{0.5}TiO_2$) and a rock-salt $LiTiO_2$ [7]. The reasons for these different structural behaviors are at present not understood. Here, with the aid of *ab initio* simulations, we aim to rationalize the phase behavior of intercalated rutile and to get insights into the underlying mechanisms.

2. Details of calculation

All calculations were performed within the framework of density functional theory as implemented in the CASTEP software, within the pseudopotential plane-wave formalism [18]. Electron exchange and correlation effects are treated within the spin polarized generalized gradient approximation [19] with ultrasoft pseudopotentials [20] used to replace the Ti (1s, 2s, 2p), O (1s), and Li (1s) core orbitals. This set-up results in calculated cell parameters within 1% from the experimental values for undoped rutile. The calculations were performed on supercells containing up 16 formula units of TiO_2, which was found to be of sufficient size to predict the intercalation behavior of various titanate structures [10,21,22]. All degrees of freedom, including internal ionic positions and the size and shape of the computational unit were fully optimized in simulations. In order to quantify the distribution of electron den-

* Tel.: +44 2076790488; fax: +44 2076790488.
E-mail address: mkoudriachova@msn.com

0378-7753/$ – see front matter © 2011 Elsevier B.V. All rights reserved.
doi:10.1016/j.jpowsour.2010.12.081

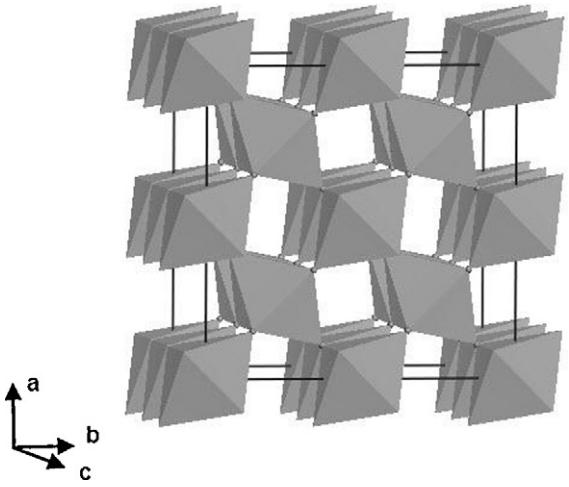

Fig. 1. Polyhedral representation of the structure of rutile.

sity donated to the host lattice upon intercalation and to monitor the changes in ionic charges, Mulliken population analysis was performed. The spatial orientation of the charge donated to the Ti-ions was monitored by visualizing the distribution of the charge density in t_{2g}-orbitals as described in Refs. [10,23].

3. Results and discussion

3.1. Li-intercalation into bulk rutile

Rutile is built from pillars of TiO_6 octahedra, in which each octahedron shares two opposite edges. The pillars are joined by corners to form a tetragonal structure with straight channels along the tetragonal axes (the *c*-direction) (Fig. 1), where intercalated lithiums can be accommodated in vacant interstitial sites. In polycrystalline rutile Li-ions are inserted along the *c*-direction and have a high mobility along *c*-channels [9,10,24,25]. The ordering of Li-ions in bulk rutile has been studied by Koudriachova et al. [9,10]. It was shown that deformations of the local structure of the host, induced by intercalation, cause Li-ions to order themselves in the *ab*-planes rather than adopt configurations maximizing their separations under electrostatic repulsions [26]. A very slow diffusion of Li-ions in the *ab*-planes in bulk rutile restricts access to stable configurations, and thus limits the insertion concentration [9].

Detailed analysis of the fully relaxed configurations of lithiated structures performed here suggests that the ordering pattern of the Li-ions in the bulk, which plays such important role in intercalation behavior of rutile, is a direct consequence of insufficient separation between the inserted Li^+-ion and the neighboring Ti^{4+}-ions. Strong Coulomb repulsions with the inserted Li-ions pushes neighboring Ti-ions away from their crystallographic positions into the *c*-channels, increasing the Ti–Ti separation in the occupied site (from 4.6 Å in undoped rutile to 5.14–5.17 Å), but reducing the available space in the neighboring vacant sites. The resultant local deformations affect the ability of the vacant sites to insert Li-ions upon further intercalation. Here we use Ti–Ti distances across the insertion site to characterize this ability: the vacant sites with the reduced separations compared to the bulk are less favorable for Li-insertion, while more spacious vacant sites become more favorable. As an example, a fully relaxed configuration at [Li]/[Ti] = 0.0625 is shown in Fig. 2, where the Li-ion adopts an asymmetric position at (0.25*a*, 0, 0.134*c*), which locally breaks the tetragonal symmetry, The sites with the largest Ti–Ti separations (4.92–4.95 Å) are labeled as *B* and *C*, the sites with a modest expansion as *D* and *E* (4.78 Å), while sites labeled *A*, which neighbor the occupied site in the *a*- or *b*-direction are closed in, to 4.18 Å (4.23 Å). Therefore, at [Li]/[Ti] = 0.125 occupation of the most "open", *B* and *C*, sites is preferred, as it is confirmed by direct calculations. However, the displacements of Ti-ions affect transport of inserted Li-ions to these sites along the *c*-channels, in addition to limited accessibility due to slow diffusion in the *ab*-planes [9]. Li-migration through the "closed" sites hinders the accessibility of the *B*-, *E*- and, in particular, the *C*-sites, where the barrier is in excess of 1 eV. In comparison, all Ti–Ti distances across the *c*-channels with *D*-sites are larger than in bulk rutile (4.62–4.75 Å). As a result, population of the less favorable, but more accessible *D*-site at higher Li-concentrations is more likely.

At higher concentrations ([Li]/[Ti] = 0.125–0.75) the most stable configurations are formed upon occupation of both *B* and *D* sites [10] and the accessibility of the *B*-sites is improved at higher Li-concentrations, after a collective lattice expansion in the *b*-direction. Geometric considerations suggest that the *C*-sites would be occupied if superstructures with maximum Li-separation are formed at $x > 0.25$. Therefore, slow diffusion of Li-ions along the "closed" *c*-channels makes formation of such superstructures in bulk rutile infeasible.

A direct consequence of the edge sharing motif of rutile is that electronic charge transferred to the host upon intercalation is accommodated in localized R-d_{yz}-orbitals (in the notation from Ref. [23]) of the Ti-ions, causing locally an elongation of the Ti–O bonds along the *z*-direction (apical bond) of the local frame of reference (i.e. in the *ab*-planes) and an overall volume expansion [23]. The deformations of the TiO_6 octahedra associated with the displacements of the Ti-ions reshape these orbitals as shown in Fig. 2A. In the "deformed" octahedra only one apical Ti–O bond is elongated to the Ti^{3+}–O^{2-} value (by 10–12%) and tilted to the local equatorial (*xy*-)plane, while the second apical Ti–O bond is contracted (by approximately 10%). As the overall volume expansion at $x \sim 0.0625$ and 0.125 is predicted to be much smaller (1–2%), such deformations clearly minimize the volume expansion as the charge donated to the host lattice is accommodated and, therefore, will be favorable under the volume relaxation constraints. Since reduction of Ti-ions to their 3^+-state and elongation of all six bonds to the Ti^{3+}–O^{2-} values occurs upon accommodation of one donated electron, elongation of one bond, as shown in Fig. 2A is expected at $1/6\,|e|$. *Ab initio* calculations show that Li-ions donate $-0.82\,|e|$ to the lattice, hence this electron charge will be donated at Li-concentration of ~0.2 [Li]/[Ti], which is an estimate for the upper boundary of single phase insertion in bulk rutile, in excellent agreement with that observed experimentally [2] and predicted earlier using *ab initio* simulations [10]. The above simple considerations represent an "averaged" picture of the charge distribution. The exact distribution depends of course on the ordering of Li-ions as, through elongation of the particular Ti-O bonds, it supports the structural distortions required for accommodation of the Li-ions. Each Li-ion neighbors six Ti-ions, with two of them being displaced as described above (and receiving $\sim -1/6\,|e|$ each). Assuming for the sake of simplicity that the rest of the charge is distributed uniformly among the remaining Ti-ions, it is easy to see that at ~0.2 [Li]/[Ti] all Ti-ions receive $\sim 1/6\,|e|$ each, validating the "averaged" description at these concentrations. The restriction on Li-concentration in the single phase domain under the current scenario is also evident from counting the sites available for intercalation. As each Ti-ion neighbors four insertion sites, reduction of two Ti-ions per inserted Li precludes occupancy of seven sites around them. It is easy to check that in the cell used here for computation ($Li_xTi_{16}O_{32}$) these considerations yield a maximum occupancy of 3 Li per 16 Ti-ions, i.e. ~0.2 [Li]/[Ti].

Upon further intercalation, the single phase insertion is followed by a two phase insertion, whereby a tetragonal rutile phase coexists with the monoclinically distorted rutile with an ordering of Li-ions

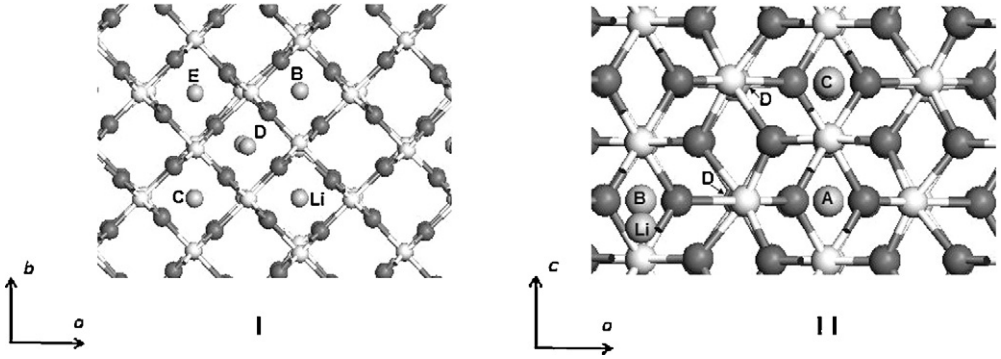

Fig. 2. A fully relaxed configuration of $Li_{0.0625}TiO_2$. The non-equivalent vacant insertion sites are marked by A–E. I: top view; II: side view.

in alternating *ab*-layers with filled and half-filled interstitial *B* and *D* sites [17]. The electronic mechanism for this phase transformation is discussed in Ref. [23]. In the monoclinic phase, the charge donated by the lithiums is accommodated in d_{xy}-orbitals, while the *R*-d_{yz}-orbitals are empty. Comparison of the computed energies shows that two phase insertion is only slightly favorable over single phase insertion in this concentration domain (by 0.02 eV per formula unit at $x = 0.5$). However, two phase insertion is favored by kinetics as the ordering of Li-ions in the coexisting phases is very similar, while ordering in the single phase at intermediate concentration differs considerably [10]. Full occupancy of the d_{xy}-orbitals is expected upon accommodation of $-2/3$ $|e|$ (i.e. upon elongation of 4 out of 6 bonds to the Ti^{3+}–O^{2-} value); this corresponds to [Li]/[Ti] ≈ 0.8. At higher Li-concentrations the donated charge is accommodated in hybridized orbitals and the structure transforms into a layered hexagonal phase, which has a distorted rock-salt structure with a special ordering of Li-ions [17]. The above structural behavior is excellent agreement with that observed experimentally [2].

In nanostructured rutile a large proportion of Ti-ions reside in surface and sub-surface regions, which are structurally different from bulk rutile and are partly reduced. The increased flexibility in accommodating distortions associated with charge donation, and a less restricted volume expansion lead to a shift of the boundary of the single phase domain to higher insertion concentrations, as observed in Ref. [4]. In case Li–Ti distances in the parent structure are increased (for instance, in very small nanoparticles due to the surface tension, or upon doping by a suitable dopant) the ordering in the single phase domain also will be less pronounced and the limitations imposed by diffusion in the single phase domain will be further relaxed. It is possible that in very small nanoparticles Li-insertion will occur in a single phase at all insertion concentrations. Similarly, the presence of defects such as heteroions will affect the phase boundaries as observed in Refs. [28,29].

3.2. Li-intercalation into spaghetti-like nanoparticles

The morphology of spaghetti-like nano-particles, which have their axis along the *c*-direction, brings considerable modifications in the above intercalation behavior. First of all, a small cross section [4,7] results in enhanced diffusion in the *ab*-planes. Also, spaghetti-like nanoparticles intercalate Li-ions predominantly through the walls, i.e. along the *a*- or equivalently *b*-directions. Consequently, Li-occupation in the *ab*-planes is not restricted and the "bottle-necks" at the closed sites in the *c*-channels are not relevant. In addition, expansion in the *ab*-planes is less constrained than in the bulk, so that the boundary of the single phase insertion domain is shifted to higher Li-concentrations. Under a less constrained volume expansion, two Ti–O bonds are elongated to the Ti^{3+}–O^{2-} value as shown in Fig. 2B, instead of one Ti–O bond in the bulk. To elongate 2 Ti–O bonds to the Ti^{3+}–O^{2-} value $-1/3$ |e| needs to be transferred, giving an estimate for the upper concentration of the single phase domain as 0.45 [Li]/[Ti]. At these Li-concentrations the preferred single phase configuration in the bulk has alternating filled (with *B* and *D* sites occupied) and empty *ab*-layers [11,18]. The single phase configuration is only slightly less favorable than coexistence of the two phases discussed above.

As the Li-concentration increases, screening of Li-interactions by local distortions becomes less efficient [10], especially if the preferred ordering is disrupted (for instance, at elevated temperature and near the surface). These repulsions push Li-ions away from each other to maximize their mutual separations, causing occupancy of sites *C* rather than sites *D* (Fig. 3). The typical distance allowing for screening of Coulomb interaction of Li-ions with an ionic charge of ~0.8 $|e|$ in titanates is about 3 Å [22].

The distortions associated with such occupancy are depicted schematically in Fig. 4 for the structure corresponding to occupation of the *C*-sites at [Li]/[Ti] = 0.125. The "displaced" Ti-ions are essentially five-fold coordinated, with the bonds to the oxygen ions marked as O1-ions broken (Ti–O1 distance 2.49 Å), bonds to the oxygen ions labeled as O2 elongated to the T^{3+}–O^{2-} value (2.05 Å), and remaining bondlengths shortened to 1.83–1.92 Å. If the "displaced" Ti-ions migrate further into the vacant interstitial space, as indicated by the arrows, to rebind with the oxygen array, and Li-ions rearrange themselves in the emerging spaces, the structural connectivity becomes reminiscent of that of spinel structured titanates, which are more stable than lithiated rutile at the Li-concentration range 0.34–05 [Li]/[Ti] (by 0.05 eV at [Li]/[Ti] = 0.5). It has been shown previously that stability of spinel structured Li-titanates is based on a regular network of four-fold coordinated Li-ions [22], which is formed as Li-ions distribute themselves in the

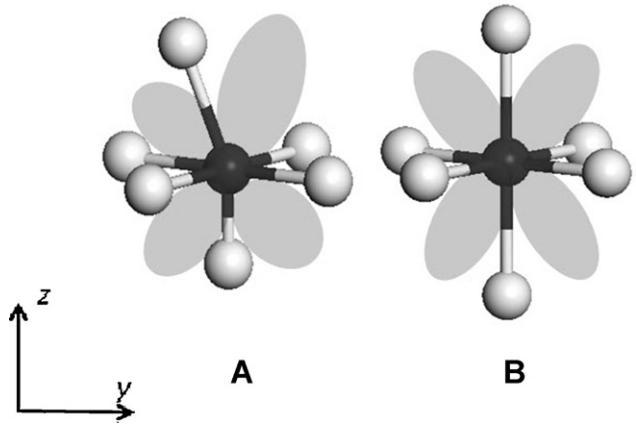

Fig. 3. The shape of the *R*-d_{yz}-orbitals in a constrained (A) and an unconstrained (B) lattice expansion in the *ab*-planes after intercalation of Li-ions. The *c*-direction is perpendicular to the plane of the picture.

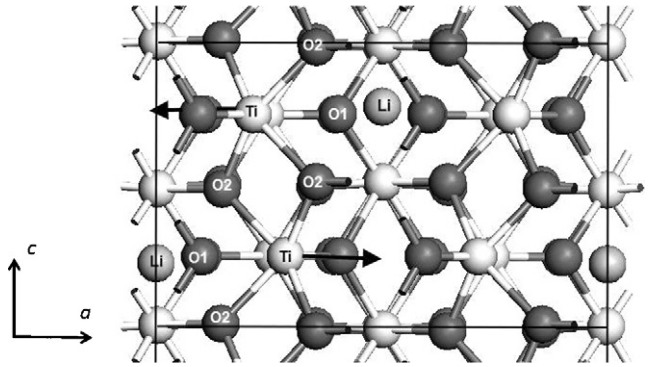

Fig. 4. Displacements of Ti-ions towards interstitial sites in configurations maximizing separation between the Li-ions. The labeling of O-ions is explained in the text.

structure so as to maximize their separations. In the spinel structure the spacing between Li-ions is about 3 Å, and TiO_6 octahedra are deformed to provide each Li-ion with a 4-fold coordination to neighboring O-ions. The charge donated to the host is accommodated in hybridized t_{2g}-orbitals that stabilize the distortions of TiO_6 octahedra [22]. Upon further intercalation, spinel $Li_{0.5}TiO_2$ transforms to rock salt $LiTiO_2$. The detailed discussion of the mechanism underlying this transformation can be found in Ref. [22].

A phase transformation to spinel has been observed upon heating of another lithiated titanate, orthorhombic $Li_{0.5}TiO_2$, which is obtained upon lithiation of anatase structured TiO_2 [27].

As the phase transformation to spinel occurs when the thermodynamically favorable ordering of Li-ions is disrupted, it can be expected at elevated temperature for a wide range of (nanostructured) transition metal oxides at approximately 0.5 Li per transition metal.

4. Conclusions

Using *ab initio* simulations we have shown that nanoparticles of rutile of a special shape (spaghetti-like) can display a phase behavior distinctly different from that of the bulk or nanostructured rutile. On the nano-scale the boundary of the single phase reaction, displayed at low Li-concentrations in the bulk, shifts to higher Li-concentrations enabling an alternative structural evolution upon intercalation. As Li-ions strive to form a regular network at these concentrations, rutile undergoes a transformation to a spinel phase, while intercalation into bulk rutile leads to formation of monoclinically distorted Li-rutile. At elevated temperatures a transformation to a spinel phase is expected for a wide range of intercalated (nanostructured) transition metal oxides.

Acknowledgments

This research was funded by the EPSRC under grant nos. EP/C545222 and EP/C54521.

References

[1] B. Zachau-Christiansen, K. West, T. Jacobsen, S. Atlung, Solid State Ionics 28–30 (1988) 1176.
[2] W.J. Macklin, R.J. Neat, Solid State Ionics 53–56 (1992) 694.
[3] M.A. Reddy, M.S. Kishore, V. Pralong, V. Cainaert, U.V. Varadaraju, B. Raveau, Electrochem. Commun. 8 (2006) 1299.
[4] E. Baudrin, S. Caissaignon, M. Koelsch, J.-P. Jolivet, J.-M. Tarascon, Electrochem. Commun. 9 (2007) 337.
[5] D.H. Wang, D.W. Choi, Z.G. Yang, V.V. Viswanathan, Z.M. Nie, C.M. Wang, Y.J. Song, J.G. Zhang, J. Liu, Chem. Mater. 20 (2008) 3435.
[6] H. Qiao, Y.W. Wang, L.F. Xiao, L.Z. Zhang, Electrochem. Commun. 10 (2008) 1280.
[7] M. Vijayakumar, K. Sebastien, K. Rosso, J. Liu, J. Hu, J. Phys. Chem. C 113 (2009) 14567.
[8] C.H. Jiang, I. Honma, T. Kudo, H.S. Zhou, Electrochem. Solid State Lett. 10 (2007) A127.
[9] M.V. Koudriachova, N.M. Harrison, S.W. de Leeuw, Phys. Rev. Lett. 86 (2001) 1271.
[10] M.V. Koudriachova, S.W. de Leeuw, N.M. Harrison, Phys. Rev. B 65 (2002) 235423.
[11] M.A. Reddy, M.S. Kishore, V. Pralong, U.V. Varadaraju, B. Raveau, Electrochem. Solid-State Lett. 10 (2007) A29.
[12] M.V. Koudriachova, ECS Trans. 16 (42) (2009) 63.
[13] A.R. Armstrong, G. Armstrong, J. Canales, R. García, P.G. Bruce, Adv. Mater. 17 (7) (2005) 862.
[14] M.V. Koudriachova, J. Nano Res. 11 (2010) 159.
[15] F. Jiao, P.G. Bruce, Adv. Mater. 19 (2007) 657.
[16] D. Munoz-Rojas, E. Baudrin, Solid State Ionics 178 (21–22) (2007) 1268.
[17] M.V. Koudriachova, S.W. de Leeuw, N.M. Harrison, Chem. Phys. Lett. 371 (2003) 150.
[18] CASTEP 3.9 Academic Version, Licensed under the UKCP-MSI Agreement, 1999.
[19] J.P. Perdew, Phys. Rev. B 34 (1986) 7406.
[20] D. Vanderbilt, Phys. Rev. B 41 (1990) 7892.
[21] M.V. Koudriachova, Chem. Phys. Lett. 458 (2008) 108.
[22] M.V. Koudriachova, Phys. Chem. Chem. Phys. 10 (33) (2008) 5094.
[23] M.V. Koudriachova, N.M. Harrison, S.W. de Leeuw, Solid State Ionics 175 (2004) 829–834.
[24] O.W. Johnson, Phys. Rev. A 136 (1964) 284.
[25] M.V. Koudriachova, N.M. Harrison, S.W. de Leeuw, Solid State Ionics 157 (2003) 35.
[26] M.V. Koudriachova, N.M. Harrison, S.W. de Leeuw, Comput. Mater. Sci. 24 (2002) 235.
[27] R.J. Cava, D.W. Murphy, S. Zahurak, A. Santoro, R.S. Roth, J. Solid State Chem. 53 (1) (1984) 64.
[28] M.V. Koudriachova, N.M. Harrison, S.W. de Leeuw, MRS Proc. 756 (2003) 149.
[29] H. Uchiyama, E. Hosono, H. Zhou, H. Imai, Solid State Ionics 180 (2009) 956.